Meteor Radar Study of Ionospheric Wind at Kyoto

By

Takehiko ASO*, Toshitaka TSUDA*, Yoshio KARASAWA**, Shoji MATSUDA***, Yoshio YONEDA****, Yosuke TAKASHIMA***, Rei ITO*, Toru NONOYAMA* and Susumu KATO*

(Received Februdry 8, 1979)

Abstracts

This paper describes the results of meteor radar observations which have been carried out at Kyoto University since December, 1977. The radar, a coherent pulse doppler radar with a transmitting frequency of 31.57 MHz and a nominal peak power of 10 kW, is able to detect wind fields at meteor regions of 80-110 km. The solar semidiurnal tide generally dominates the wind oscillations at these heights, while a diurnal tide of comparable magnitude reveals itself in a less regular manner. Some anomalies in the amplitude and phase characteristics of the tides are shown, which might be related to a possible interaction with winds and waves, or to some disturbed conditions in the earth's atmosphere. Also planetary scale waves such as quasi-2-day oscillations and resonantly magnified gravity-mode waves have also been found there. Hence, the meteor radar, together with its cooperation with other observations, will helps us understand the dynamical process of atmospheric waves on a global scale.

1. Introduction

The meteor radar at Kyoto University (34°51'N, 136°6'E) has been operating since December, 1977[1]. It detects echo returns from ionized trails produced by impinging meteors in the 80-110 km height region of the upper atmosphere. The echo doppler shift reveals the neutral wind field which comprises the prevailing wind, planetary-scale wave, tidal wave and fluctuating components such as internal gravity wave and turbulence. From these observations, we could obtain information on the dynamical process including excitation, propagation and interaction of waves in the earth's upper and lower atmosphere under various conditions. The usual meteor radar

* Ionosphere Research Laboratory, Faculty of Engineering
** Now at the Kokusai Denshin Denwa Co., Ltd.
*** Now at the Nippon Electric Co., Ltd.
**** Now at the NHK Corporation

Table 1 Parameters of the Kyoto University meteor radar system.

Site	Shigaraki, Shiga (34°N, 136°E)
Type	Coherent Pulse Doppler Radar
Items	Echo Amplitude
	Range
	Doppler Shift
	Azimuth & Elevation
Frequency	31.57 MHz
Peak Power	10 KW
Pulse Width	280 μsec with 10 μsec×28 bits
	Code Modulation
Repetition	Variable (Max. Duty 10%)
Arrival Angle	Interferometer/Decay Height Method
Range	Pulse Compression Method
Receiver Dynamic Range	Greater than 50 dB
Aerial	5-element Yagis
Radar Control	On-line Small Computer
Data Taking	Real-time Processing and Recording
	onto Magnetic Tapes
Remarks	Mobile on board a Trailer

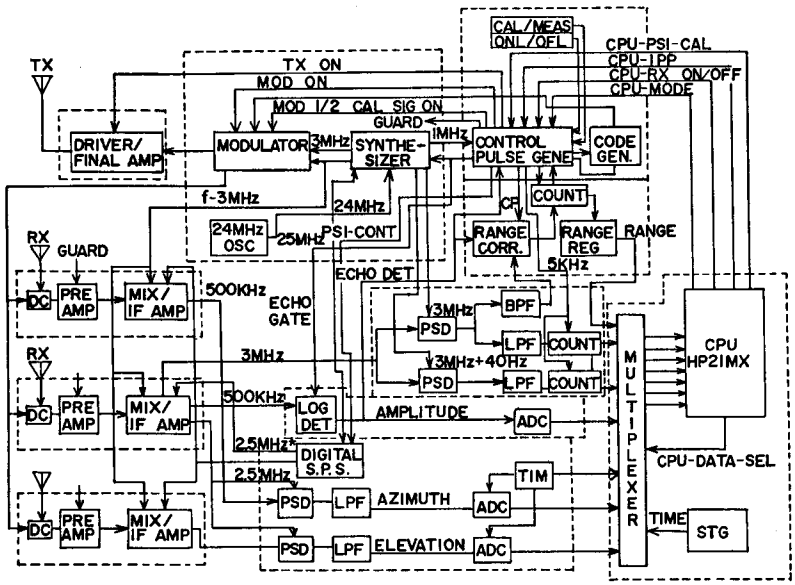

KYOTO UNIVERSITY METEOR RADAR SYSTEM

Fig. 1. Blockdiagram of the Kyoto University meteor radar.

with moderate echo rates is preferentially suited for tidal and longer period studies, though a synoptic study of short period components is also possible. The data base presented here represents almost a full year of the latest observations covering the URSI/IAGA CTOP campaign participated in by the GRMWSP network sponsored by IAGA[2].

2. Equipment

Some significant parameters of the radar system are listed in Tab. 1. The radar is a monostatic, coherent pulse doppler radar, whose basic idea has descended from the Mark-II system, recommended as the international prototype by the IUCSTP in 1971[3]. Several improvements and originalities are incorporated in the new system.

Fig. 1 illustrates the block diagram of the whole system. A pulsed CW signal of

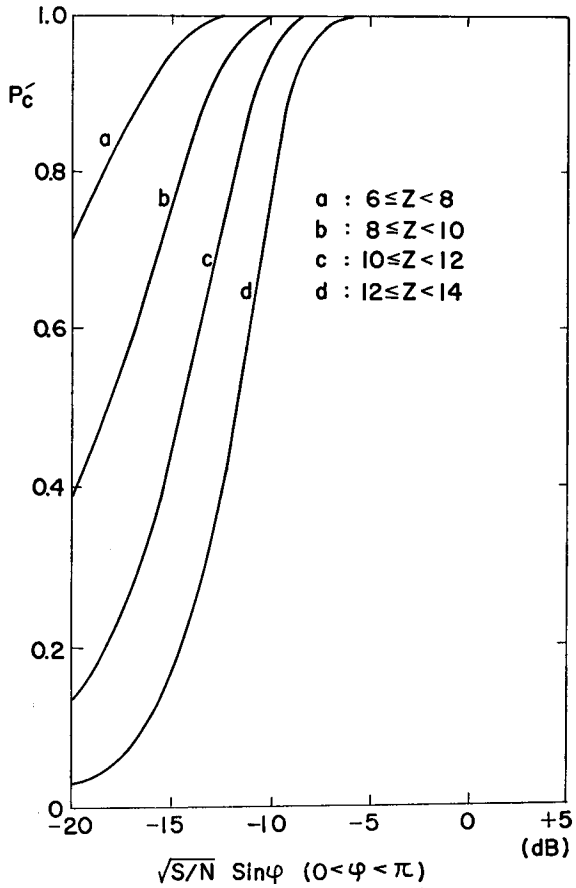

Fig. 2 Range detection probability as a function of narrowband signal-to-noise ratio. Z is range correlator threshold.

10 KW peak power is transmitted at a frequency of 31.57 MHz. The pulse width is 280 μsec with a 90° phase keying every 10 μsec by a 28 bits pseudo random code. Hence, the transmitted signal is equivalent to the superposition of a 280 μsec long, narrowband (7kHz) pulse and a 10 μsec bit length phase reversed wideband (200kHz) pulse. The echo range is determined by the pulse compression technique[4]. A range correlator for a code modulated signal gives a range mark with a resolution of 1.5 km. Fig. 2 shows the probability of detecting correct range marks versus a narrowband signal-to-noise ratio $(S/N)_n$ times phase factor relating to the round trip for various values of the correlator threshold. After 10 modulated pulses the transmitter returns to the unmodulated narrowband pulses in order to improve the signal-to-noise ratio for the doppler shift and angle detection subsystems. The echo doppler shift, corresponding to the line of the sight velocity of drifting meteor trails, is retrieved by two channel baseband detectors of 0 and 40 Hz offset with clock frequencies of 625 Hz and 5 kHz, respectively. An error for the typical values of the line-of-sight velocity derived from the 40 Hz offset system is estimated to be less than 0.5 m/sec for a single echo, whose duration is longer than 0.2 sec with $(S/N)_n$ exceeding 10 dB. In this case, the receiver gate width is 400 μsec for an interpulse period of 5 msec. (Fig. 3) The echo amplitude is measured with a dynamic range of more than 50 dB

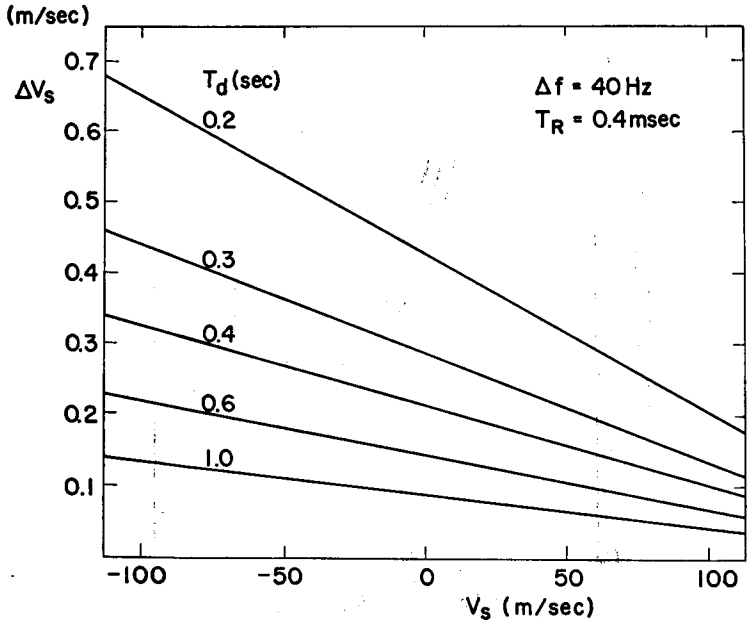

Fig. 3 Error in line-of-sight velocity measurements for various values of echo duration.

using a logarithmic amplifier. The sky noise temperature at the radar site is about 10000 K. Hence, minimum sensitivity of echo detection lies around -110 dBm, and the threshold $(S/N)_n$ is about 10 dB. An echo return exceeding the threshold sets the echo flag to initiate the observation sequence.

The arrival angle of an echo is determined by spaced antenna phase comparisons, using the phase sequenced interferometer scheme developed by the Durham group[5]. This method was also recommended by the IUCSTP. A digitally controlled stepwise

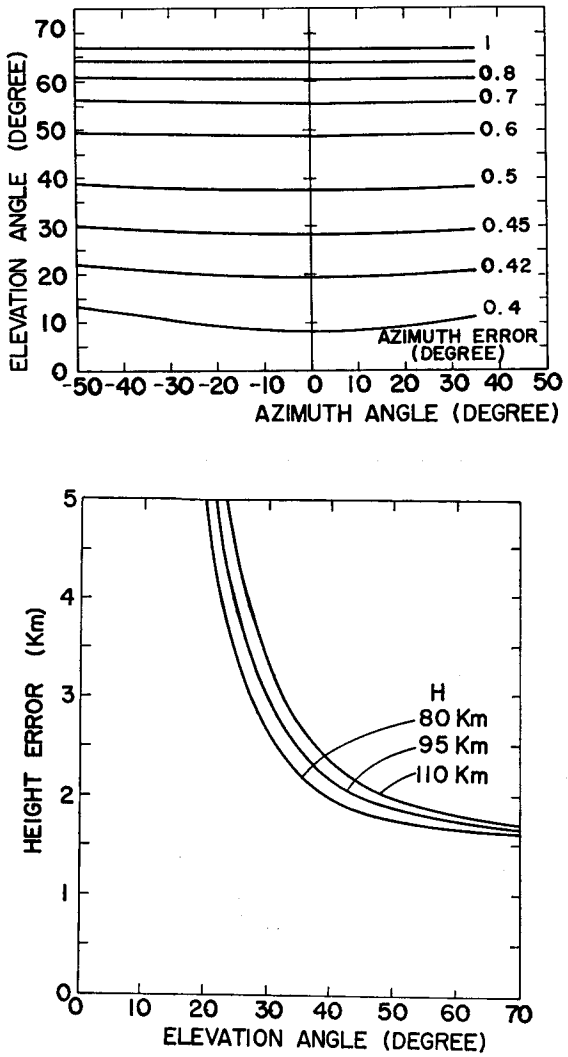

Fig. 4 Errors in (a) height as a function of elevation and (b) in azimuth as a function of both elevation and azimuth.

phase scanning circuit was designed. Phase differences for both echoes and calibration signals are determined with a sequence of 11 pulses. Two nearly orthogonal baselines with an approximate two wavelength spacing are used for the elevation and azimuth finding systems. An error in height determination as a function of elevation and also an error in azimuth as a function of both elevation and azimuth are illustrated in Figs. 4 (a) and (b), respectively. In this estimate, $(S/N)_n$ is set to 10 dB. It is shown that the azimuthal error is less than 0.5° and that the height determination error is less than 1.5–3 km for most of the echoes entering into the main lobe of the receiving antennas. At present, the absolute height calibration of the system remains to be done, so the data to be presented here was analysed assuming decay height conventions.

A digital computer supervises the whole system, including radar control, echo vali daiton and real time analysis. Observations are taken for 200 pulses when a significant echo is detected. The radar then returns to the "watch" mode, where the pulse repetition frequency is reduced to a fraction of that of the "measure" mode. A 1627-word record is written on a magnetic tape after each pulse. More than 6000 echoes can be stored on one magnetic tape. The off-line processing was carried out at the Data Processing Center of Kyoto University.

3. Observations

Fig. 5 shows specimen records of (a) the A-scan display of an echo and a range correlator output, and (b) slow scan records of an underdense-type echo with doppler

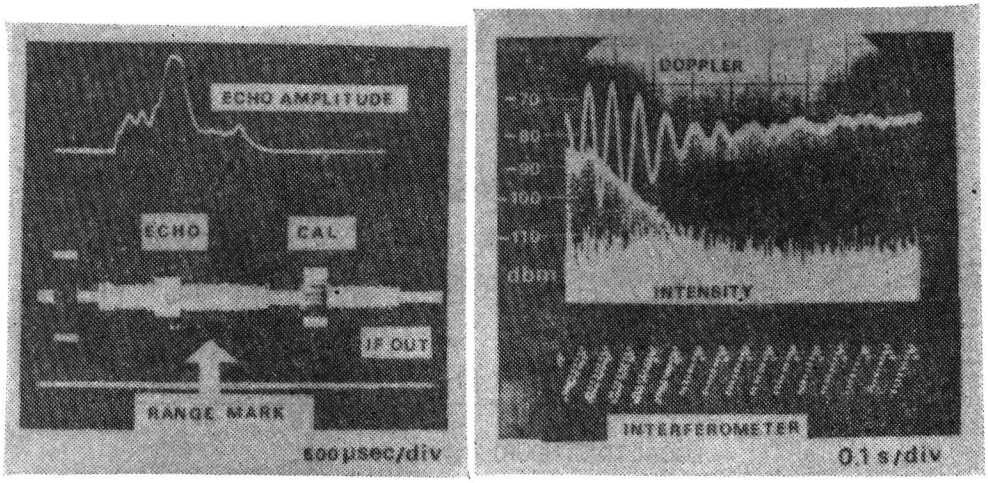

Fig. 5 Specimen records of (a) the A-scan display of echo and range correlator output and (b) slow scan display of underdense-type echo, doppler shift and interferometer waveforms.

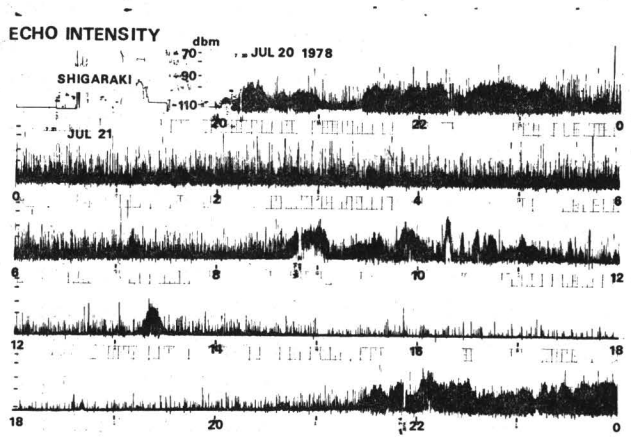

Fig. 6 Full-day record of echo returns on 20 July 1978.

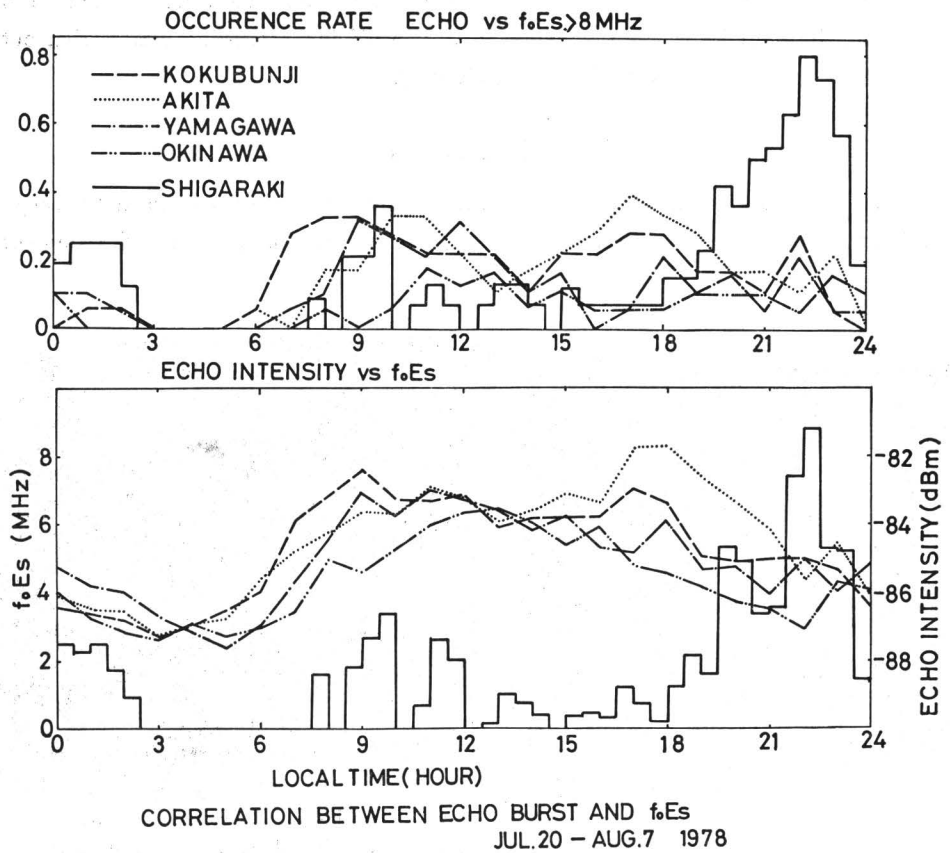

Fig. 7 Correlation of long enduring echo with f_0E_s relating to occurence rate and intensity.

shift and interferometer waveforms. Spurious range marks appear in Fig. 5 (a) due to noises which can be eliminated through pulse-to-pulse correlation. In the slow scan display, Fig. 5 (b), the echo amplitude exhibits a discontinuity after the first ten pulses due to the code modulation. The echo decays exponentially in 0.3 sec after the echo recognition. The height inferred from this decay rate is about 96 km. The doppler channel with a zero offset frequency shows a doppler shift of 14 Hz while the echo exceeds the noise level. This gives a line-of-sight velocity of 60 m/sec for the 31.57 MHz operating frequency. The interferometer output gives stepwise waveforms, alternating between echo and calibration when the echo is present.

Fig. 6 shows the record of echo returns for more than 1 day in July, 1978. Impulsive echoes which frequently appear from midnight to morning are normal meteor trail echoes with durations less than 1 sec. Occasionally, burst signals are distinguished by their long lasting enhancement of echo intensity. These bursts have range values corresponding to E layer heights. The occurence rate and intensity of the burst echo, averaged between Jul. 20-Aug. 7, exhibit a weak correlation with f_oE_s observed more than 400 km distant from the site. (Fig. 7) But the diurnal variation indicating double hump maxima is very similar to those of the 50 MHz Es patterns of the summer months shown by Dyer[6]. This backscatter is presumably produced by some kind of sporadic E which is attributed to field-aligned irregularities at temperate latitudes.

Fig. 8 shows a continuous plot of an underdense-type echo distribution for the

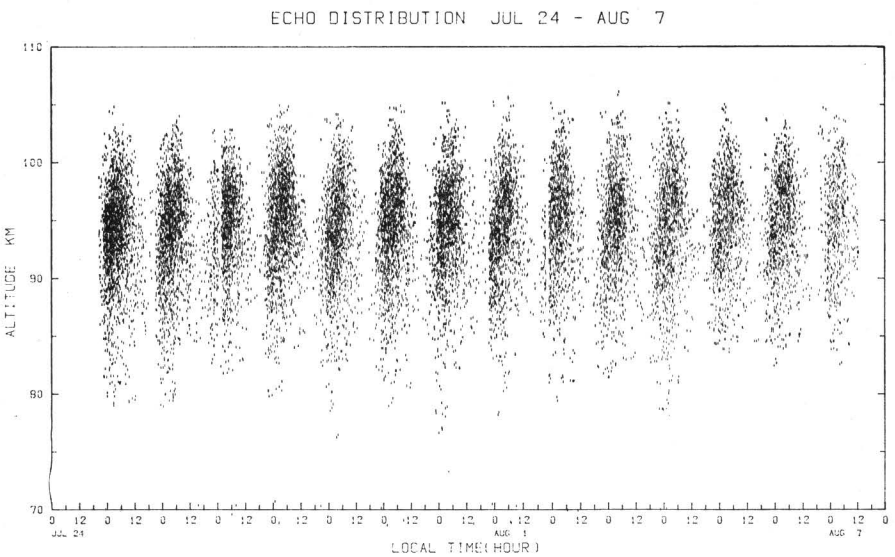

Fig. 8 Echo distribution versus altitude and local time for the summer CTOP period in 1978.

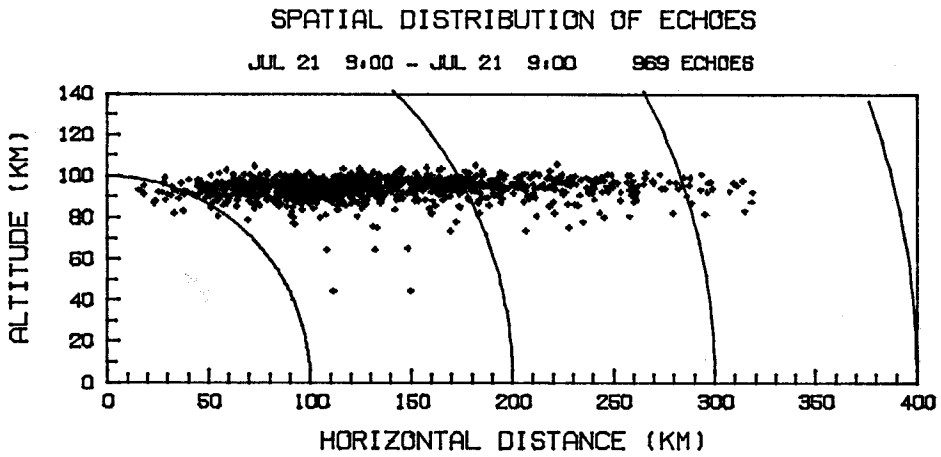

Fig. 9 An example of spatial distribution of echoes on 21 July 1978.

period of the CTOP campaign run, Jul. 24–Aug. 7. The average echo rate amounts to 1.5×10^3 per day with a maximum hourly rate of about 150 around 0600 LT and a minimum around 1800 LT. The average decay height of the echoing region is found to show some descent around 1800 LT. This is probably related to the diurnal variation of atmospheric parameters. An increase in the density or a decrease in the temperature reduces the decay rate, causing a lower virtual height to be inferred. The maximum deviation in the virtual height from the decay rate method is of the order of several kilometers in the meteor zone. In Fig. 9, there is also plotted an echo distribution in the vertical plane. Most of the echoes arrive in the direction with an elevation angle ranging over 25°–65°.

Antennas were directed to the north for most of the observations. The measured wind velocities are assumed to correspond to a component in the direction that the antenna was pointing, as the azimuth measurement system still lacks absolute calibration. The error introduced by the finite beam width of the receiving antenna is to underestimate the meridional component by about 10%, and to augment the variance of deduced wind values due to a contaminating zonal component. The situation will soon be improved with the completion of calibrating interferometer direction finding system.

The wind system in the meteor zone is tabulated in Tab. 2. The prevailing wind conforms to a mean wind of a single station averaged over several days. The planetary wave has been linked to a tropospheric weather system and is observed at times at meteor heights[7]. Atmospheric tides are one of the most important wave phenomena in this region[8]. These long period waves are propagated from below or are excited there by in-situ solar radiation or dynamical coupling processes. The global nature of these

Table 2 Wind system in the meteor zone.

	Magnitude (m/s)	Period	Horizontal scale (km)	Vertical scale (km)	Note
Prevailing winds	10-20	≫days	global	10-20	
Planetary waves	10-20	several days	global down to 1000*	50	*linked to tropospheric weather system
Tides	5-40	several-24 hours	global	>20	
Internal gravity waves	10	1-several hours	40-several hundreds	10	
Turbulence	30?	*several tens of minutes	1-several hundreds	0.1-5?	averaged decay time

long period oscillations requires cooperative observations on a world-wide scale. Internal gravity waves as well as turbulence have a comparatively small scale in time and space, and are subject to a synoptic study as shown by Justus and Woodrum[9]. Some of them are intimately related to magnetic and weather disturbances.

In our meteor radar observations, the hourly rate of useful meteor trails normally varies from several to several hundreds, randomly occuring over a horizontal extent of several hundred kilometers in the altitude range of 30 km centered at around 90-95 km. To facilitate the inference of wind components from single station observations, we assume that the motions are predominantly horizontal, with a horizontal scale much larger than the sounding region and a period of oscillation longer than the sampling interval of the meteor trails at a particular height. Thus, in the following analysis, we will concentrate on the oscillations with tidal and longer periods. Since atmospheric tides and planetary waves are periodic in time and longitude, wind fields can be decomposed to a time harmonic factor with respect to local time, multiplied by some vertical structure function which, in the classical tidal theory, is independent of latitude[10]. If the tide is migrating, the phase of each component is independent of the longitude where the observations are made. The decomposition of the wind field into mean and tidal components is carried out using the least square fitting proposed by Groves[11], where the vertical function for each time harmonic, quadrature component is assumed to be polynomial in altitude. Also employed is the Fourier spectrum analysis in discussing non-tidal oscillations.

4. Results

Fig. 10 shows the spectrum analysis of the wind velocity for 15 full days of observations during 19 consecutive days in 1978. The power spectra are obtained for the

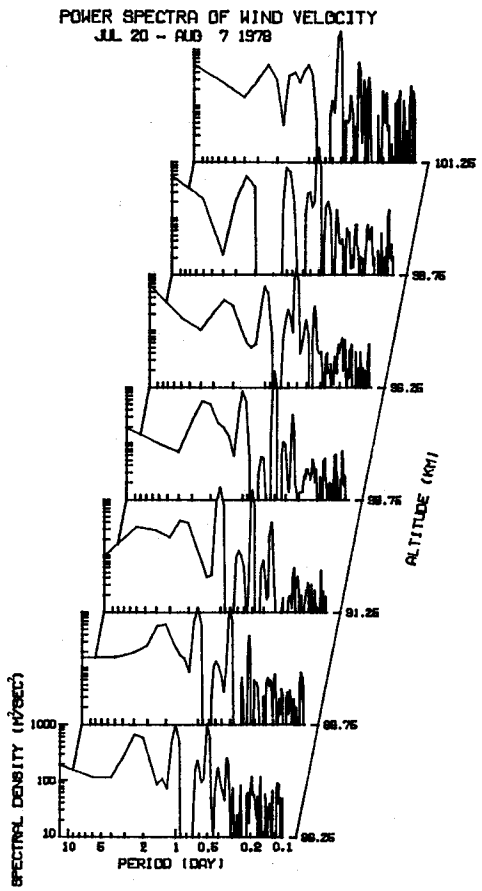

Fig. 10 Power spectra of wind velocity for the 2.5 km altitude interval in the same period as in Fig. 8.

height interval of 2.5 km by the Blackman-Tukey algorithm with a maximum lag of 6 days. The results indicate a steady peak at the semidiurnal period, while a diurnal component of comparable magnitude is also seen. This agrees with the theoretical prediction that the migrating diurnal tide prevails at lower latitudes. A well-marked peak around 48 hrs might correspond to a quasi-2-day planetary-scale wave which is observed to dominate in the summer meteor zone.[12),13)] The peak at around 8 hrs corresponds to the terdiurnal component. It must also be noted that the peaks at 10 or 14 hrs might correspond to resonantly magnified gravity-mode waves[14)]. Further discussions will be treated elsewhere.

A contour illustration of the slowly varying component in the same period is shown in Fig. 11. In the figure, wind values are digitally filtered by a low-pass filter whose

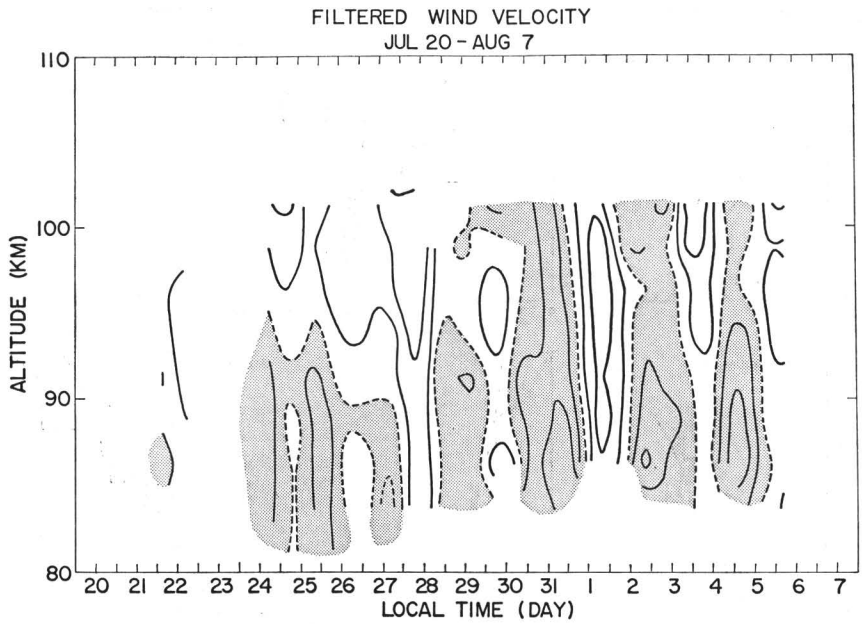

Fig. 11 Contour plot of slowly varying component for the same period as in Fig. 8. The contour levels are 10m/sec, and shaded contours represent southward.

cut-off period lies around 32 hrs. The contour levels are 10 m/sec and the shaded contours represent southward components. The results show appreciable day-to-day variations. On the average, however, the prevailing wind is southerly at heights above 90 km where more than 80% of the observations were made. The reverse flow from the summer to winter hemishpere is observed at lower altitudes qualitatively consistent with the middle atmosphere general circulation model, though the reversal occurs at slightly higher altitudes. A quasi-2-day oscillation detected by the spectral analysis is evident in the latter half period with its amplitude exceeding some 20 m/sec. The phase indicates a downward progression, and the inferred vertical wavelength is very long, consistent with the nearly evanenscent nature of planetary waves in this region.

Fig. 12 shows the wind structure of mean, diurnal and semidiurnal components obtained by the Groves method for assumed polynomial height variations of order 1, 2 and 3, along with the time-wise fitting for the prescribed height spacing of 3 km (hatched squares). The phase of diurnal and semidiurnal components is the local time at northward maximum. It is seen that the polynomial representation of order 2 or greater can describe the wind variation. Some 24500 echoes were analyzed to deduce the diagram. Both the diurnal and semidiurnal components show a downward phase progression, and, accordingly, an upward propagation of wave energy. The phase of

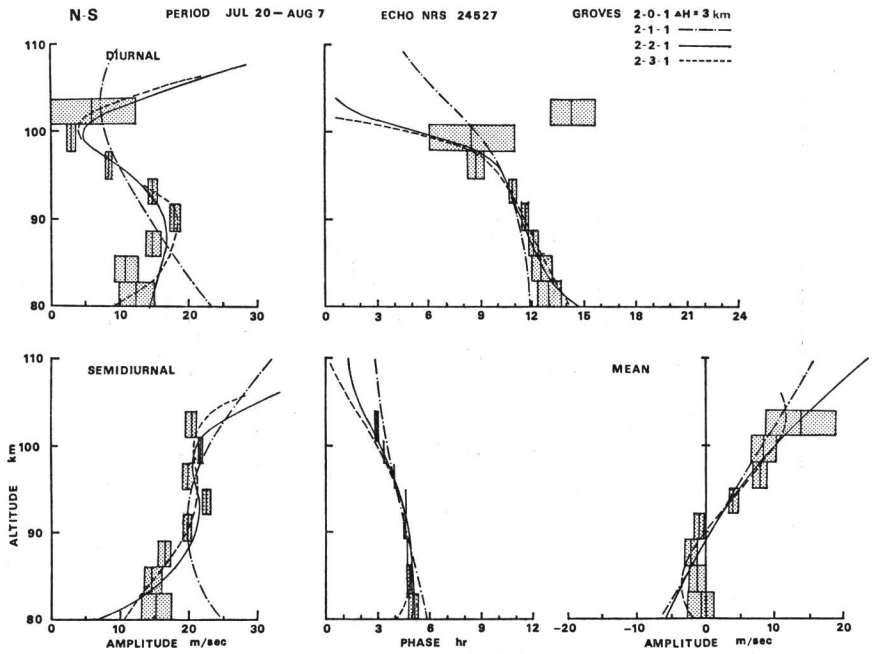

Fig. 12 Structures of mean, diurnal and semidiurnal winds for the same period as in Fig. 8.

the diurnal component between 85-95 km lies around 1100-1300 LT, consistent with that of Greenhow and Neufeld[15]. At around 100 km, the diurnal oscillation diminishes, followed by an irregular phase change. The semidiurnal component is roughly constant and 20 m/sec in the 85-105 km height. Its phase is significantly definite and 0400 LT at 96 km with a slight increase with height. This agrees quite well with other published data and theoretical predictions for summer conditions which indicate the presence of fundamental (2, 2) mode. The mean wind corresponds basically to the averaged feature of those given in Fig. 11.

A comparison of north-south and east-west wind components by changing the antenna pointing direction on May 4-6 is given in Fig. 13. For the diurnal oscillation, the zonal amplitude is larger than the meridional up to 100 km. The phase of the zonal component lags by about 4 hours, indicating a clockwise rotation of the velocity vector around a tilted ellipse. The phase of each component shows an unusual variation: a merging and, presumably, a dissipation of upward and downward (reflected or in-situ excited) waves occur at 92-94 km. Probably, in association with this, a very large value of westward wind is observed at slightly higher altitudes. This might suggest that the atmospheric tides contribute to the induction of zonal winds in the lower thermosphere[16]. These phenomena might have a link to some magnetically disturbed

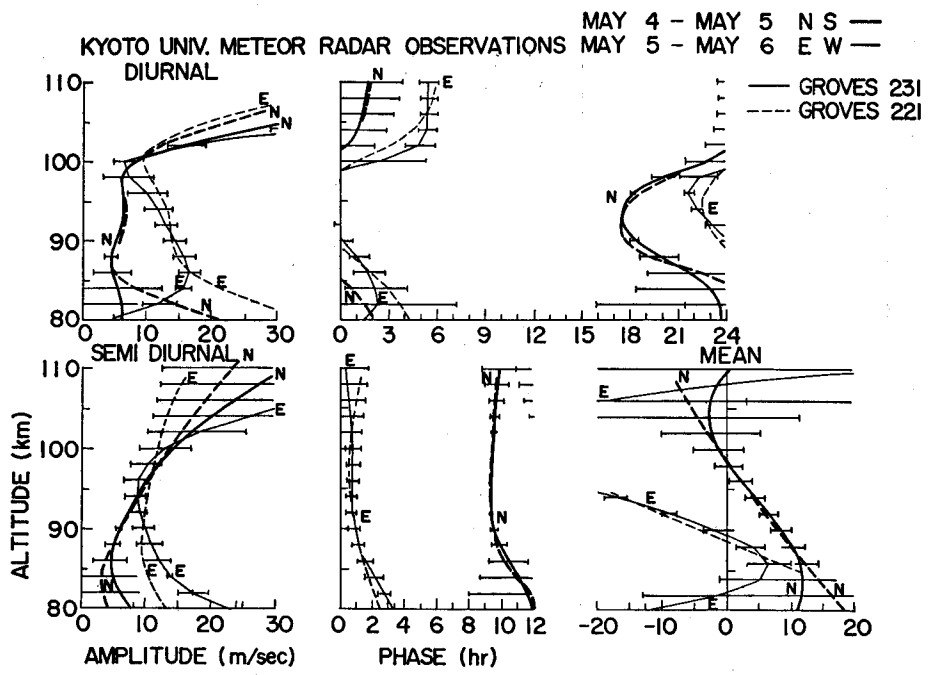

Fig. 13 Same as Fig. 12 for 4-6 May 1978.

condition where $\sum K_p > 45$ on May 1-4. For the semidiurnal component, the phase lag is closely equal to 3 hours at all altitudes with 0930 LT above 90 km for the meridional component. Its amplitudes are of comparable magnitude in the altitude range of 90-100 km. Thus, the polar plots of a semidiurnal wind at 35°N are almost circular, and rotating clockwise consistent with the classical theory[17]. A vertical spectral analysis will show up vertical wavenumbers of pertinent tidal modes. Mean winds of 7 m/sec northward and 15 m/sec westward were inferred at these heights.

The north-south components for each observation run during June and July are illustrated in Figs. 14(a) and (b). In June, appreciably variable wind structures are indicated. June 21-23 and 26-28 and 26-28 show a dominant semidiurnal wind, while during July 7-10, which corresponds to a CTOP period, the diurnal wind dominates. As is stated by many workers, the variability is ascribed to a variable forcing, a temperature structure and a background flow. Hence, critical study of the results should be forwarded from the viewpoint of a global atmospheric coupling. July's results seem to be more stable and the phase of the semidiurnal component is well-defined as is already seen in Fig. 12.

An averaged structure of diurnal and semidiurnal components for the summer CTOP campaign run is compared with various theoretical and experimental results in

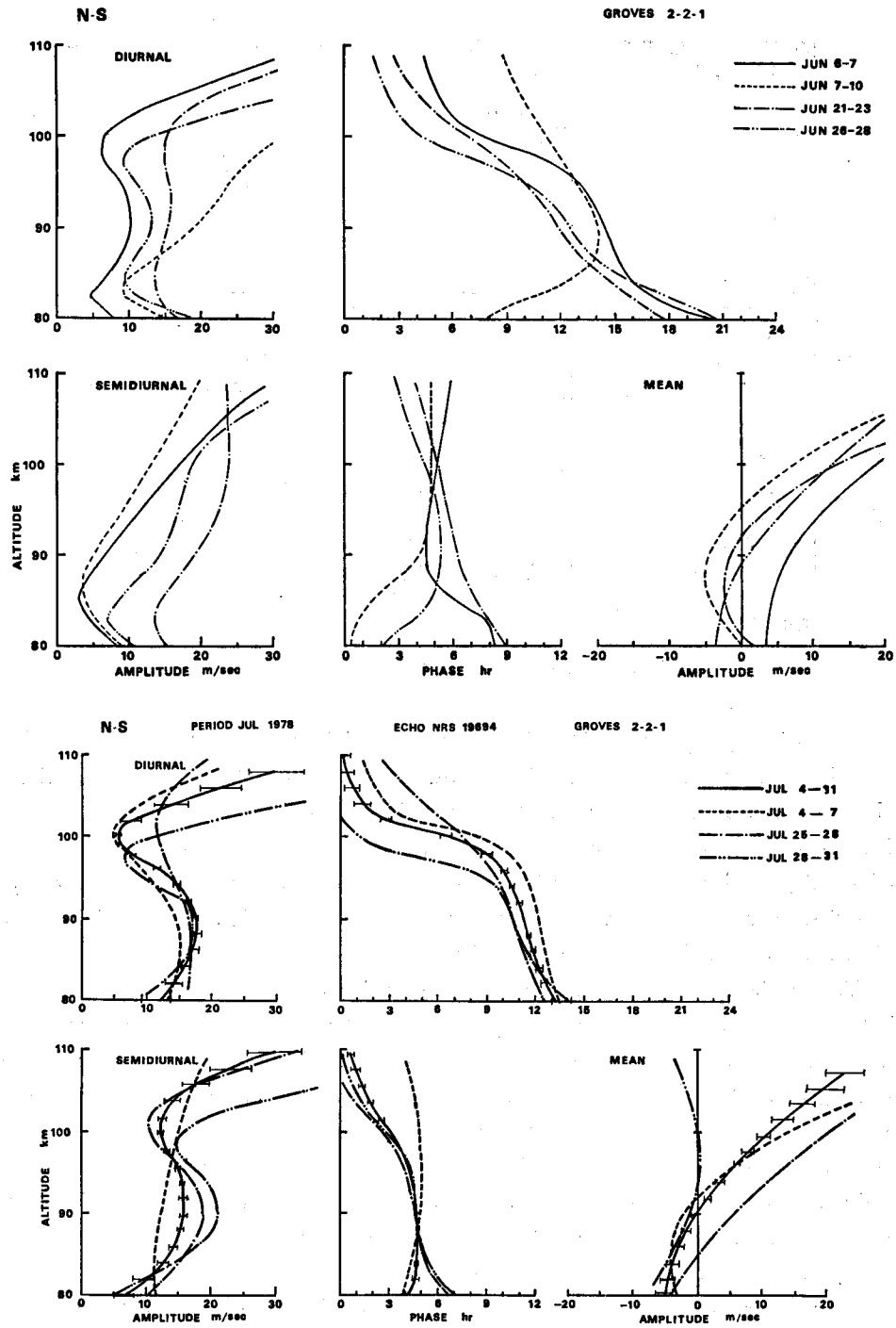

Fig. 14 Same as Fig. 12 for (a) June (b) July 1978.

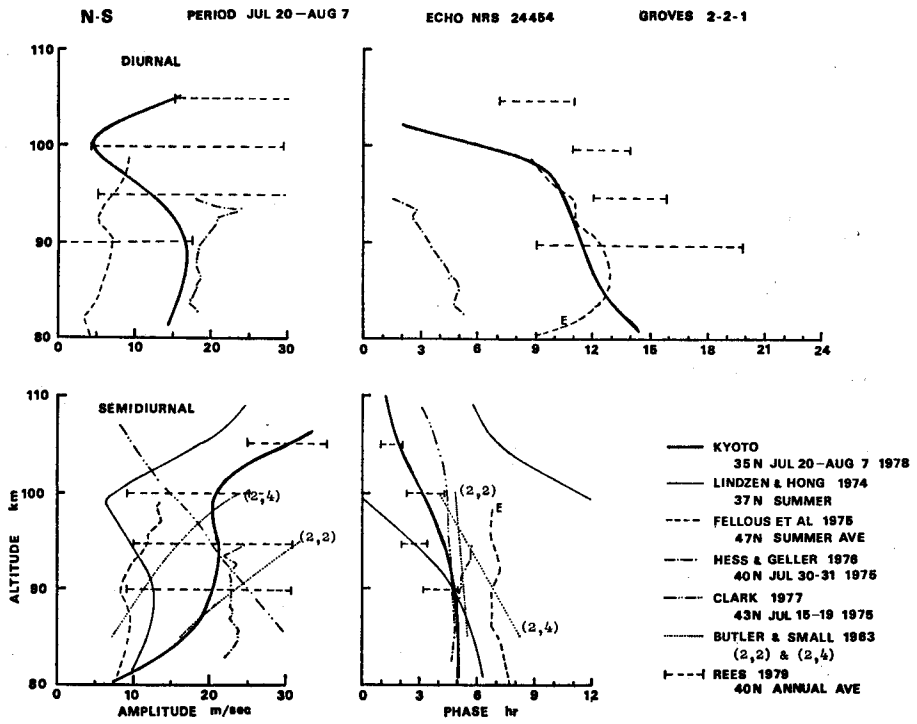

Fig. 15 Comparisons of averaged structure for the CTOP period with other tidal studies.

Fig. 15[17),18),19),20),21),22)]. Only the results of Fellous et al.[17)] are for the zonal wind. The diurnal phase differs appreciably from Hess and Geller's[18)] but lies near the annual average obtained from a chemical release experiment aboard rockets.[19)] For the semidiurnal component, the classical theory of Butler and Small[20)] and an improved work by Lindzen and Hong[21)] compare well in its general feature with our results. Meteor observations by us together with Fellous et al.[17)], Hess and Geller[18)] and Clark and Wand[22)] for different latitudes are also consistent with averaged rocket results. The phase of our result might adequately be explained by the (2, 2) mode. The variability involved in the wave process, however, renders its straightforward interpretation somewhat complicated.

The result of an equinoctial observation in September is shown in Fig. 16. In the figure, the average over two periods, September 13-14 and 19-22, is augmented by hatched squares as in Fig. 12. Observations and theorectical predictions for equinoctial conditions are shown with reference to tidal components. On Sept. 13-14, the diurnal component, especially its phase below 100 km, is well reproduced by Lindzen's theory[10)], and indicative of a predominating (1, 1) mode. The phase merges with that of Forbes and Garret[23)] above 100 km. On Sep. 19-22, however, the null in amplitude

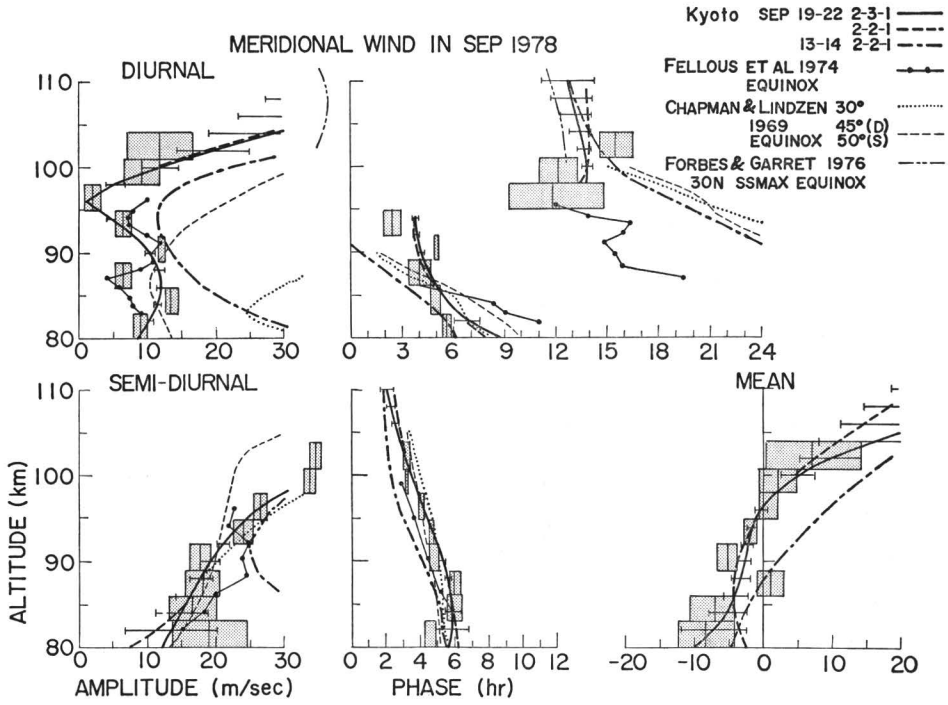

Fig. 16 Same as Fig. 12 for September 1978.

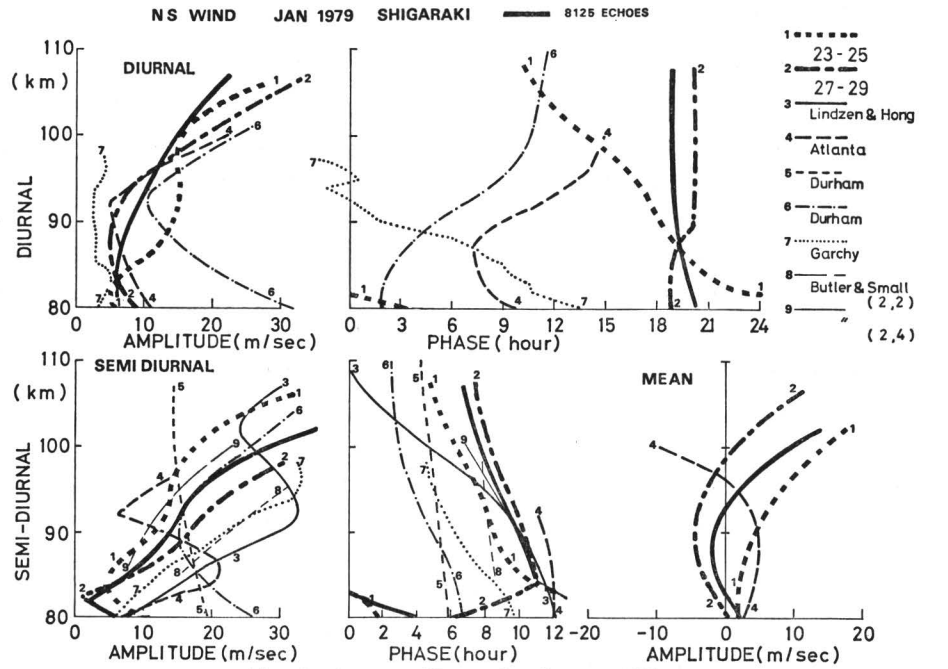

Fig. 17 Same as Fig. 12 for January 1979.

at 96 km is more clearly seen, associated with a rapid phase change which is a significant result because of the high echo concentration there. In this case, the phase progression is slower with the altitude above and below the reversal region, and suggests a standing wave structure due to the presence of partially reflected or in-situ excited diurnal waves. For the semidiurnal tide, our result is definite and well explained by Lindzen's classical theory where the ozone drive is predominantly of (2, 2) mode. The mean prevailing wind is not largely different from those in June and July.

Fig. 17 illustrates the winter observations of January, 1979. The solid line represents the mean of two periods denoted by 1 and 2, and other profiles numbered 3 through 8 are reference data in winter[16),20),21),24),25)]. There exists a noteworthy variation with every observation and every period. For the semidiurnal tide however, the structure can be delineated by the theoretical (2, 4) mode. This agrees with the pre-

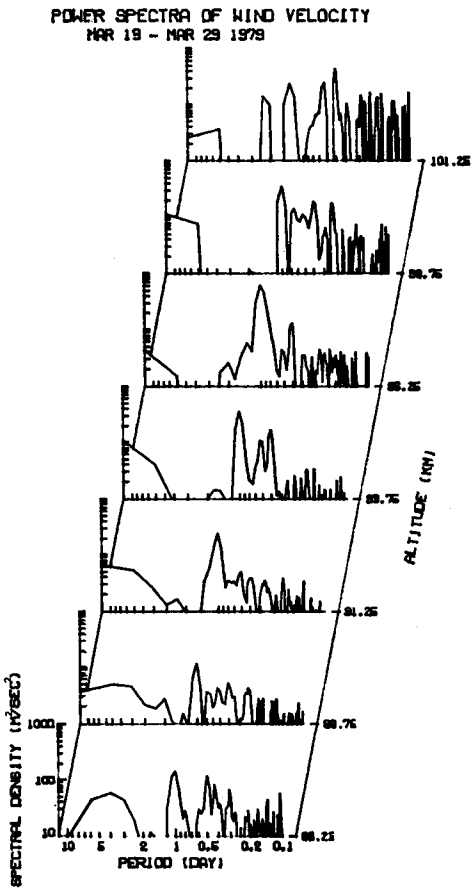

Fig. 18 Same as Fig. 11 for the spring CTOP period in 1979.

valence of the higher order (2, 4) mode in winter season as is pointed out by Harper[26].

Results for the vernal equinox observations are given in Fig. 18. These power spectra are calculated for the CTOP period of 13-26, March, 1979. The results indicate a remarkable decrease of long period components including quasi-2-day oscillations compared with the summer data in Fig. 10. Also, the semidiurnal tide diminishes to a great extent compared to the diurnal one, which is rather usual in spring[27]. These facts again strongly suggest the possible influence on tidal and other atmospheric waves effected by the background mean flow and thermal structure.

A harmonic dial representation of the monthly mean diurnal and semidiurnal tide is given in Fig. 19, where the phase variation with altitude is also averaged out. The dotted pattern is the seasonal average produced by the Sheffield group through many years of observations at 50-53° of north latitude[27]. The agreement is rather good in December, March, and June through August, but not in April, May or September. In January, however, it must be recalled that the latitudinal structure of the dominant (2, 4) mode implies the possibility of a phase reversal between two stations. The diurnal component shows a large scatter in contrast to Muller's results, where both the NS and EW components maximize between 14-16 LT. It may not be appropriate to discuss the short vertical wave length diurnal tide on an averaged harmonic dial.

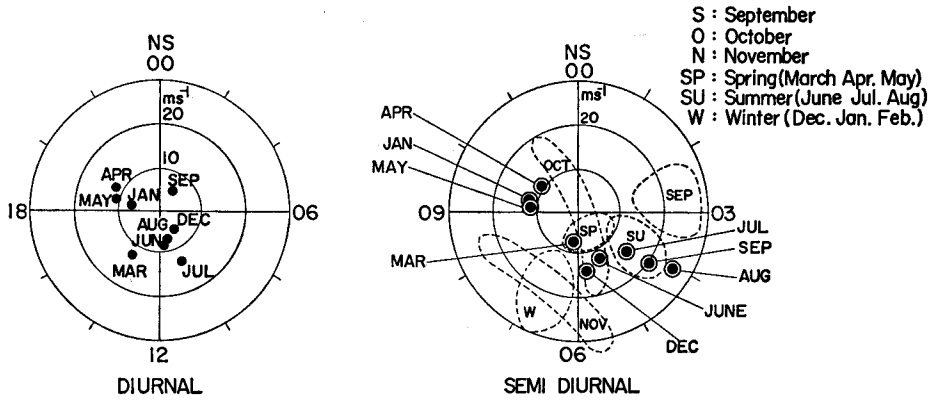

Fig. 19 Harmonic dial for monthly averages for December 1977- January 1979.

5. Summary and conclusions

A brief description of the system and the results of almost a full year of observations of the Kyoto meteor radar are presented. It is shown that the radar can reveal mean winds, the diurnal and semidiurnal tides, quasi-2-day planetary waves and some kind of gravity waves in the mid-latitude meteor region. These results suggest a strong dynamical coupling of the winds and waves in the whole region of the earth's atmos-

phere. Hence, an organized cooperation of observing networks is indispensable for a better understanding of the profound atmospheric dynamics.

References

1) Aso, T., T. Tsuda and S. Kato: J. Atmos. Terr. Phys. **41**, (1979), in press.
2) Roper, R. G. and A. Woodman: J. Atmos. Terr. Phys. **40**, 879 (1978).
3) Barnes, A. J. Jr: Bull. Am. Meteorol. Soc. **54**, 9, 900 (1973).
4) Nowak, R., E. M. North and M. S. Frankel: Final Rep. SU-SEL-70-021, Stanford Univ., Stanford, Calif. (1970).
5) Glanz, F. H.: IEEE Trans. Geosci. Elec. GE-9, 56 (1971).
6) Dyer, P. J: Radio Sci. **7** (3), 351 (1972).
7) Muller, H. G: Phil. Trans. R. Soc. Lond. A. 271, 585 (1972).
8) Kato, S.: Space Sci. Rev. **12**, 421 (1971).
9) Justus, C. G. and A. Woodrum: T. Atmos. Sci. **30**, 1267 (1973).
10) Chapman, S. and R. S. Lindzen: Space Sci. Rev. **10**, 3 (1969).
11) Groves, G. V.: J. Atmos. Terr. Phys. **16**, 344 (1959).
12) Muller, H. G. and L. Nelson: J. Atmos. Terr. Phys. **40**, 761 (1978).
13) Glass, M., J. L. Fellous, M. Massebeuf, A. Spizzichino, I. A. Lysenko and Yu. I. Portniaghin: J. Atmos. Terr. Phys. **37**, 1077 (1975).
14) Giwa, F. B. A.: Quart. J. R. Met. Soc. **95**, 771 (1969).
15) Greenhow, J. S. and E. L. Meufeld: Quart. J. R. Met. Soc. **87**, 472 (1961).
16) Miyahara, S: J. Meteor. Soc. Japan, **56**, 86 (1978).
17) Fellous, J. L., R. Bernard, M. Massebeuf and A. Spizzichino: J. Atmos. Terr. Phys. **37**, 1511 (1975)
18) Hess, G. C. and M. A. Geller: Aeron. Lab., Dep. Elec. Eng., Univ. Ill., Urbana-Champaign.
19) Rees, D.: J. Geomag. Geoelect. **31**, (1979), in press.
20) Butler, S. T. and K. A. Small: Proc. Roy. Soc. **A274**, 91 (1963).
21) Lindzen, R. S. and S-S Hong: J. Atmos. Sci. **31**, 1421 (1974).
22) Clark, R. R. and R. H. Wand: Contribution to IAGA/IAMAP Assembly, Seattle, Aug. 1977.
23) Forbes, J. M. and H. B. Garret: J. Atmos. Sci. **32**, 1976).
24) Roper, R. G.: J Atmos. Terr. Phys. **40**, 891 (1978).
25) Clark, R. R.: ibid, 905 (1978).
26) Harper, R. M.: Prirate communication.
27) Muller, H. G.: Planet. Space Sci. **14**, 1253 (1966).